Journal of the Ceramic Society of Japan 134 [11] 792–799 2026
DOI https://doi.org/10.2109/jcersj2.26050

JCS–Japan

FULL PAPER

Structure and acid-resistance of dissolution–precipitation reaction products formed on β-tricalcium phosphate particles after fluoride treatment

Satoshi Hayakawa[1,†], Ryoma Aoki[2], Noriyuki Nagaoka[3], Takuya Kataoka[1] and Tomohiko Yoshioka[1]

[1] Faculty of Interdisciplinary Science and Engineering in Health Systems, Okayama University, 3–1–1 Tsushima-naka, Kita-ku, Okayama 700–8530, Japan
[2] Graduate School of Interdisciplinary Science and Engineering in Health Systems, Okayama University, 3–1–1 Tsushima-naka, Kita-ku, Okayama 700–8530, Japan
[3] Advanced Research Center for Oral and Craniofacial Sciences, Okayama University Dental School, 2–5–1 Shikata-cho, Kita-ku, Okayama 700–8558, Japan

We investigated the structure and acid resistance of dissolution–precipitation reaction products obtained through fluoride treatment of β-tricalcium phosphate (TCP) particles using two types of fluoride-containing acetic acid (Ac)-sodium acetate (AcNa) buffer solutions with or without added pyrophosphate (PP) ions. X-ray diffraction and nuclear magnetic resonance spectroscopic analyses confirmed that fluoride promotes dissolution–precipitation reactions on the surface of β-TCP in fluoride treatment solutions, resulting in the formation of fluorine-substituted hydroxyapatite (F-HAp) and calcium fluoride (CaF_2). In this dissolution–precipitation reaction in acidic solutions with high fluoride concentrations, hydrolysis of β-TCP and precipitation of spherical CaF_2 particles occurred, resulting in the formation of raspberry-like aggregates covering the surface of the β-TCP. Subsequently, rod-shaped F-HAp particles formed in the gaps between CaF_2 particles and at the interface between CaF_2 particles and β-TCP particles. The addition of PP ions in the fluoride treatment solution inhibited the hydrolysis reaction of β-TCP, and higher PP concentrations suppressed the formation of F-HAp and CaF_2. Results of the acid resistance evaluation indicated that dissolution–precipitation products of β-TCP, which was composed of a core–shell-type structure with F-HAp core and CaF_2 shell, had a decreased initial dissolution rate in Ac-AcNa buffer solutions.

Keywords: β-tricalcium phosphate, Fluoride treatment, Dissolution–precipitation, Fluorine-substituted hydroxyapatite, Calcium fluoride, Acid resistance

[Received May 29, 2026; Accepted August 25, 2026; Published online October 8, 2026]

1. Introduction

Topical fluoride is used in clinical dentistry to prevent dental caries.[1)] Calcium fluoride (CaF_2) is known as the primary reaction product formed on tooth surfaces after topical application.[2–5)] Recently, we investigated the effect of the deposited CaF_2 on the acid resistance of fluoride-treated hydroxyapatite (HAp) by treating commercially available HAp particles with fluoride-containing acetic acid (Ac)-sodium acetate (AcNa) buffer solutions (pH 4) with or without added phosphate ions.[6)] X-ray diffraction (XRD) and nuclear magnetic resonance (NMR) spectroscopic analyses confirmed the formation of fluorine-substituted hyrdoxyapatite (F-HAp) with the hydration layer containing calcium phosphate and CaF_2. The acid resistance of fluoride-treated HAp improved when the surface of HAp was densely covered with CaF_2 particles. On the other hand, as the concentration of phosphate ions added to the fluoride treatment solution increased, the amount of CaF_2 particles decreased, and the acid resistance of fluoride-treated HAp decreased. Since XRD and NMR analyses cannot quantitatively distinguish between HAp (starting material) and F-HAp (reaction product), the quantitative analysis of micrometer-scale structure of dissolution–precipitation products (namely F-HAp and CaF_2) and the stoichiometry of the overall reaction remains challenges.

To clarify the effect of the precipitation of CaF_2 particles on the formation of F-HAp and the micrometer-scale structure of dissolution–precipitation products, as well as the effects of these factors on the acid-resistance of the dissolution–precipitation products, in this study we applied the fluoride-treatments to polycrystalline β-tricalcium phosphate (TCP) particles as the substrates, which have a larger particle size and a smaller specific surface area (SSA) than commercially available HAp particles. β-TCP is known to have much higher solubility than HAp, and its

† Corresponding author: S. Hayakawa; E-mail: satoshi@okayama-u.ac.jp

©2026 The Ceramic Society of Japan

This is an Open Access article distributed under the terms of the Creative Commons Attribution License (https://creativecommons.org/licenses/by/4.0/), which permits unrestricted use, distribution, and reproduction in any medium, provided the original work is properly cited.

acid-resistance is expected to be significantly improved through fluoride treatment. We investigated the microstructure and acid resistance of dissolution–precipitation reaction products formed by treating β-TCP with fluoride-containing Ac-AcNa buffer solutions.

Pyrophosphates (PP) are known to inhibit the formation and crystal growth of HAp[7,8] and CaF_2.[9] Amjad reported that the affinity constant values of PP ions for the growth of HAp and CaF_2 crystals were 1.9×10^{-5} and 14.8×10^{-5}, respectively.[9] Because a higher affinity constant means a slower crystal growth rate, the PP ions can significantly inhibit the growth of CaF_2 crystals. Hence, PP ions in the fluoride treatment solution are expected to affect not only the hydrolysis reaction of β-TCP but also the acid resistance of the dissolution–precipitation reaction products. Therefore, we investigated the effect of adding PP ions to the fluoride treatment solution to inhibit the nucleation and growth of CaF_2 crystals on the hydrolysis of β-TCP, the formation of F-HAp, and the acid-resistance of the reaction products.

2. Materials and methods

2.1 Preparation of acetate buffer and fluoride treatment solutions

Solutions of Ac and AcNa (both at 0.08 mol·dm^{-3}) were mixed to prepare a 0.08 mol·dm^{-3} Ac-AcNa buffer solution. To prepare the fluoride treatment solution, an appropriate amount of sodium fluoride (NaF, Nacalai Tesque Inc. Japan) was dissolved in the Ac-AcNa buffer solution, followed by pH adjustment to reach a pH of 5.50 ± 0.02 and a fluoride ion concentration of 1.0 or 10 mmol·dm^{-3}. A characteristic feature of the products of dissolution–precipitation reactions is that they reflect the particle size and shape of the raw materials. Since β-TCP dissolves more rapidly than HAp, it was appropriate to adjust the pH of the buffer solution to 5.5 to reduce the dissolution rate of β-TCP and induce the heterogeneous nucleation and growth of CaF_2 and F-HAp on β-TCP surface. For the fluoride treatment solutions containing PP ions, sodium pyrophosphate decahydrate ($Na_4P_2O_7 \cdot 10H_2O$, Nacalai Tesque Inc. Japan) was added together with NaF into Ac-AcNa buffer solution, and the final solution had a pH of 5.50 ± 0.02, a fluoride ion concentration of 10 mmol·dm^{-3}, and a PP ion concentration of 0.001, 0.01, 0.1, 1, and 10 mmol·dm^{-3}.

2.2 Fluoride treatment of β-TCP

Commercially available β-TCP powder [$Ca_3(PO_4)_2$], (β-TCP-100, Taihei Chemical Industrial, Co. Ltd., Japan) was sieved to obtain particles smaller than 45 μm. These particles (100 mg) were added to 100 cm^3 of the fluoride treatment solution and left to stand for 2 h at 25 ± 2 °C. The suspension was then centrifuged to remove the supernatant, and then precipitate was washed with ultrapure water and dried in a thermostatic incubator at 60 °C. The fluoride-treated β-TCP samples were denoted as Fx (fluoride concentration: $x = 1$ and 10), and PyFx (PP ion concentration: $y = 0$, 0.001, 0.01, 0.1. 1.0, and 10 mmol·dm^{-3}, fluoride concentration: $x = 0$ and 10 mmol·dm^{-3}).

2.3 Characterization

The β-TCP samples before and after fluoride treatment were examined using XRD (X'pert PRO, PANalytical, Co. Ltd., Netherland) with Cu Kα radiation ($\lambda = 1.5418$ Å). The instrument was operated at 45 kV and 40 mA in the θ–2θ scan mode. A step size of 0.02° and a scanning rate of 1.00 s/step were used to obtain diffraction patterns in the range of $2\theta = 2$–70°.

The infrared spectra of the samples were recorded with Fourier transform infrared (FTIR) spectrometer (Nexus 470, Thermo-Fisher Scientific Inc., USA) with a KBr background in the wavenumber range between 1400 and 400 cm^{-1} with an accumulation time of 256 and spectral resolution of 1 cm^{-1}. Diffuse reflectance FTIR spectra of the samples diluted to 10 wt % with KBr powder were measured.

Local structures around the ^{1}H, ^{19}F, and ^{31}P atoms of fluoride-treated β-TCP samples were investigated by solid-state magic angle spinning (MAS) NMR spectroscopy. The measurements were performed under a static magnetic field of 11.7 T using an Agilent NMR DD2 500 MHz Fourier transform (FT) NMR spectrometer (Agilent Technologies, Santa Clara, CA, USA) equipped with a cross-polarization (CP)/MAS probe. The samples were packed in a zirconia rotor with a diameter of 3.2 mm. The spinning rate of the rotor at the magic angle was approximately 15,000 Hz.

^{1}H MAS NMR spectra were recorded at a resonance frequency of 499.8 MHz with a 1.15 μs pulse length ($\pi/4$-pulse) and a repetition time of 5 s. The free induction decay (FID) signals were accumulated for 60–90 pulses. Adamantane ($C_{10}H_{16}$) was used as the external chemical shift reference [$\delta(^1\text{H}) = 1.91$ ppm vs. 0 ppm for tetramethylsilane].

Local structures of ^{1}H and ^{31}P atoms close to each other were investigated by $^1\text{H} \rightarrow {}^{31}\text{P}$ CP-MAS NMR spectroscopy. These spectra were recorded at resonance frequencies of 499.8 MHz (^{1}H) and 202.3 MHz (^{31}P) with a 2.3 μs pulse length ($\pi/2$-pulse for ^{1}H), contact time of 10 ms and a repetition time of 5 s. The FID signals were accumulated for 16–471 pulses. Ammonium dihydrogen phosphate ($NH_4H_2PO_4$) was used as the external chemical shift reference [$\delta(^{31}\text{P}) = 1.0$ ppm vs. 0 ppm for 85 %H_3PO_4].

The ^{19}F MAS NMR spectra were recorded at a resonance frequency of 470.2 MHz with a 2.5 μs pulse length ($\pi/2$-pulse angle) and a repetition time of 30 s, using a DEPTH pulse sequence aimed at eliminating background resonances from the probe by phase rotation. The FID signals were accumulated for 32–2168 pulses. Fluorapatite (FAp) was used as the external chemical shift reference [$\delta(^{19}\text{F}) = -98.90$ ppm vs. 0 ppm for trichloromethane ($CFCl_3$)]. ^{19}F MAS NMR spectra were analyzed using DMFIT software to achieve quantitative decomposition and simulation including individual spinning side bands.[10]

Scanning electron microscopy (SEM) images of the samples were obtained using a field emission (FE)-SEM

(JSM-6701F, JEOL Ltd., Tokyo, Japan, accelerating voltage of 5 kV). Cross-sectional images of the sample were obtained using a FE-SEM (JSM-IT800, JEOL Ltd., Tokyo, Japan, accelerating voltage of 5 kV). The cross-section of the sample was prepared using a cross-section polisher (SM-09020CP, JEOL Ltd., Tokyo, Japan). The samples were coated with high-purity osmium for FE-SEM observation using a Neoc-STB osmium coater (Meiwafosis Co. Ltd., Tokyo, Japan).

Before measuring the nitrogen adsorption isotherms, the β-TCP samples with and without fluoride treatment were heated at 105 °C for 1 h under a helium gas flow. Then the adsorption isotherms were measured using a Micromeritics GEMINI2375 (Shimadzu Corp., Kyoto, Japan). Based on the obtained isotherms in the relative pressure range of 0.040 to 0.310, the SSA was calculated by the multi-point Brunauer–Emmet–Teller (BET) method.

CaF_2 powder was purchased from Nacalai Tesque Co. Ltd. and used as reference material in each evaluation. Commercial CaF_2 powder was denoted as c-CaF_2.

2.4 Evaluation of acid resistance of β-TCP samples with and without fluoride treatment

The β-TCP samples before and after fluoride treatment were The acid resistance was evaluated as described in our previous report.[11] Fluoride-treated β-TCP samples (10 mg) were soaked in Ac-AcNa buffer solution (100 cm^3, 0.08 $mol \cdot dm^{-3}$, pH 5.5) at 25 ± 2 °C under stirring at 430 ± 15 rpm, Ca^{2+} concentration in the solution was measured at 2-s intervals for 30 min with a pH/ion meter (F-53, Horiba, Kyoto, Japan) equipped with a composite calcium ion-selective electrode (6583S-10C, Horiba, Kyoto, Japan). The initial dissolution rate was estimated using a least-square ft of dissolution data using ta liner equation that is based on the method of Bohner et al.:[12]

$$t/y = a + bt \quad (1)$$

where t is the elapsed time [min], y is the Ca^{2+} concentration [$mg \cdot dm^{-3}$], a is the vertical axis intercept [$min \cdot dm^3 \cdot mg^{-1}$], and b is the slope. The initial dissolution rate: v [$mg \cdot (dm^3 \cdot min)^{-1}$] was calculated from the vertical axis intercept of the fitting line based on the data points from 1 to 10 min.

3. Results and discussion

XRD peaks corresponding to β-TCP (ICDD-PDF #00-09-0169) were observed in the diffraction patterns of untreated β-TCP and F1 (**Fig. 1**). A weak peak at $2\theta = 31.9°$ (red circle) derived from HAp(211) (ICDD-PDF#00-09-0432) was also observed in F1. Peaks of HAp and two other peaks at $2\theta = 28.4°$ (black circle) and 46.9° derived from CaF_2(111) and (220) (ICDD-PDF#00-35-0816) were observed in F10.

The FT-IR spectra of untreated β-TCP and fluoride-treated β-TCP samples were presented in **Fig. 2**. For untreated β-TCP samples, the ν_3 and ν_4 PO_4 bands were observed in the ranges 1119 to 944 cm^{-1} and 606 and 553

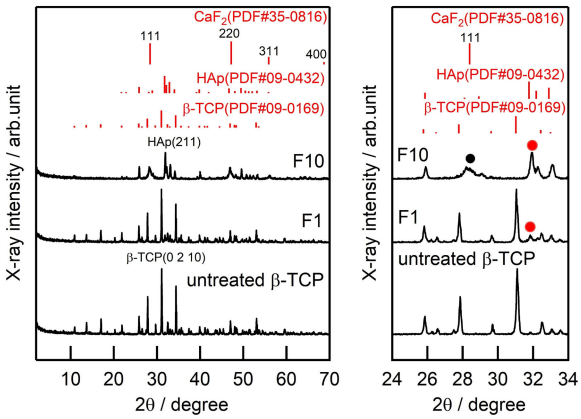


Fig. 1. Powder XRD patterns of untreated β-TCP and the hydrolysis products of β-TCP treated with fluoride-containing Ac-AcNa buffer solutions. red circle: HAp, black circle: CaF_2.

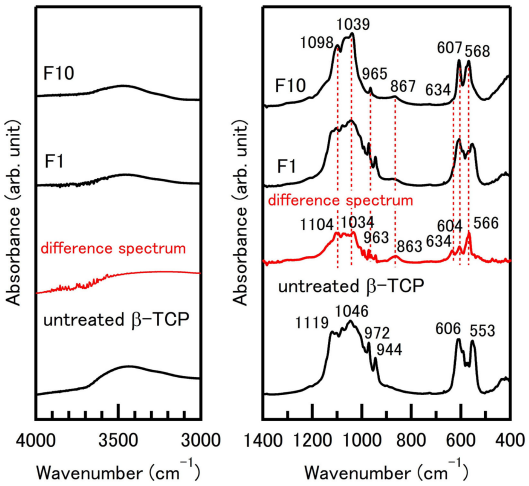


Fig. 2. FT-IR spectra of untreated β-TCP and the hydrolysis products of β-TCP treated with fluoride-containing Ac-AcNa buffer solutions.

cm^{-1}, respectively.[13] The difference spectrum obtained by subtracting the spectrum of untreated β-TCP form the spectrum of F1 matched the shape of the spectrum of F10. These spectra exhibited characteristic peaks assigned to HAp at 1098 and 1039 cm^{-1} (ν_3 PO_4), 965 cm^{-1} (ν_1 PO_4), 607 and 568 cm^{-1} (ν_4 PO_4), 634 cm^{-1} corresponding to the librational mode of OH^- ions.[14] The band at 863 cm^{-1} was assigned to the HPO_4^{2-} ions. A broad peak attributable to adsorbed water[14] were observed in the range 3700 to 3000 cm^{-1} for all samples, but no peak attributable to the stretching mode of OH groups[14] was observed at 3572 cm^{-1}. These results suggest the presence of FAp or F-HAp in the hydrolysis products of β-TCP. However, since the intensity of the IR peak derived from OH groups was extremely low, the chemical states of the OH groups and fluoride ions must be confirmed by ^1H and ^{19}F MAS-NMR.

The ^1H MAS NMR spectra of fluoride-treated β-TCP samples showed one peak at 0.1 ppm due to the OH groups in the HAp lattice, two peaks at 1.3 and 0.9 ppm due to structural water,[6] and one peak at 5.4 ppm due to adsorbed water (**Fig. 3**). The intensity of the OH group peak de-

creased in order of F1 > F10, while the intensities of structural and adsorbed water peaks followed the opposite trend. This suggests that the higher the fluoride concentration, the greater the degree of fluoridation. Untreated β-TCP exhibited a weak peak at −0.2 ppm, indicating faint traces of OH groups derived from HAp.

The ^{31}P CP-MAS NMR spectra can be deconvoluted into three symmetric peaks using a least-squares fitting algorithm (**Fig. 4**). The deconvolution results and peak assignments are summarized in **Table 1**. The spectrum of the untreated β-TCP exhibits extremely sharp peaks at 2.7, 2.8, and 2.9 ppm, corresponding to three crystallographically different PO_4^{3-} groups within the monoclinic HAp lattice. An extremely weak peak at $2\theta = 31.8°$ in the XRD pattern of untreated β-TCP can be ascribed to peaks of monoclinic HAp, suggesting that it existed as a trace impurity. This indicates that Taihei Chemical Industrial β-TCP-100 contains monoclinic HAp at the impurity level.

The ^{31}P CP-MAS NMR spectra of fluoride-treated β-TCP samples showed a broad peak at 2.8 ppm due to the PO_4^{3-} group in the hexagonal HAp lattice, accompanied by broad peaks at 1.8 and 4.7 ppm assignable to the HPO_4^{2-} and PO_4^{3-} groups, respectively (disordered phase).[6,11,15]

Figure 5 shows the ^{19}F MAS NMR spectra of fluoride-treated β-TCP samples. The broad asymmetric peak can be deconvoluted into two symmetric peaks using DMFIT software. The deconvolution results and peak assignments are summarized in **Table 2**. A sharp peak at −99.3 ppm can be attributed to F-HAp, a second peak at −104.0 ppm to CaF_2, and a third peak at −119.3 ppm to physically adsorbed F^- ions.[6,11] Since no diffraction peak corresponding to CaF_2 was observed in F1 (Fig. 1), the broad peak at −104.7 ppm can be derived from the amorphous CaF_2.

The XRD and NMR analysis results above confirmed the presence of F-HAp and CaF_2 in the hydrolysis and dissolution–precipitation reaction products of β-TCP formed

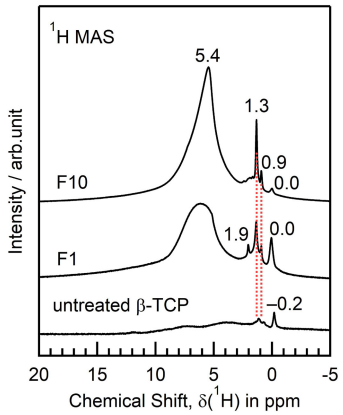


Fig. 3. ^{1}H MAS NMR spectra of untreated β-TCP and the hydrolysis products of β-TCP treated with fluoride-containing Ac-AcNa buffer solutions.

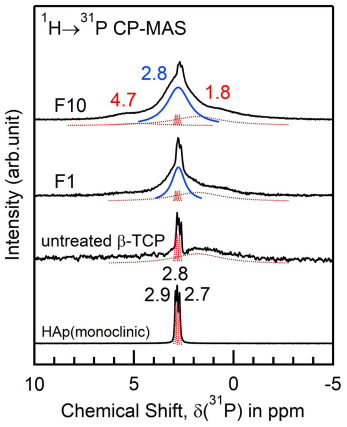


Fig. 4. ^{1}H→^{31}P CP-MAS NMR spectra of the hydrolysis products of β-TCP treated with fluoride-containing Ac-AcNa buffer solutions. For comparison, the spectrum of monoclinic HAp is also shown.

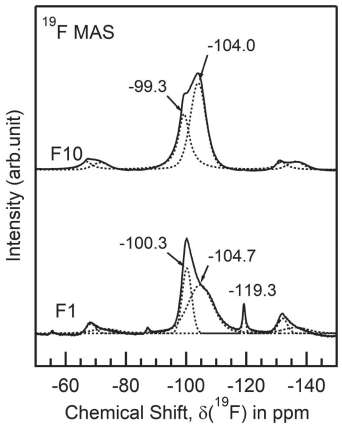


Fig. 5. ^{19}F MAS NMR spectra of the hydrolysis products of β-TCP treated with fluoride-containing Ac-AcNa buffer solutions. The deconvolution analysis results are also shown.

Table 1. Peak deconvolution analysis results of ^{31}P CP-MAS NMR spectra of the hydrolysis products of β-TCP treated with fluoride-containing Ac-AcNa buffer solutions

Sample code	PO_4^{3-}		F-HAp		HAp (monoclinic)		HPO_4^{2-}	
	Position/FWHM $\delta(^{31}P)$ in ppm	Area %	Position/FWHM $\delta(^{31}P)$ in ppm	Area %	Position/FWHM $\delta(^{31}P)$ in ppm	Area %	Position/FWHM $\delta(^{31}P)$ in ppm	Area %
F1	—	—	2.77/1.73	173.6	2.91/0.07 2.71/0.08 2.82/0.08	4.5	1.80/3.04	21.9
F10	4.75/2.46	6.1	2.77/1.36	59.5	2.91/0.07 2.71/0.08 2.82/0.08	2.8	1.80/3.04	31.6

The estimated error of chemical shifts was less than ±0.01 ppm.

Table 2. Peak deconvolution analysis results of ^{19}F MAS NMR spectra of the hydrolysis products of β-TCP treated with fluoride-containing Ac-AcNa buffer solutions

Sample code	F-HAp		CaF_2		Physisorbed F^-	
	Position/FWHM $\delta(^{19}F)$ in ppm	Area %	Position/FWHM $\delta(^{19}F)$ in ppm	Area %	Position/FWHM $\delta(^{19}F)$ in ppm	Area %
F1	−100.3/3.7	33.7	−104.7/9.7	61.6	−119.3/1.3	4.7
F10	−99.3/4.5	40.7	−104.0/6.2	59.3	—	—

The estimated error of chemical shifts was less than ±0.1 ppm.
*FAp position/FWHM (ppm): −98.9 /0.87
*CaF_2 position/FWHM (ppm): −104.5/4.07

Table 3. SSA of the hydrolysis products of β-TCP treated with fluoride-containing Ac-AcNa buffer solutions

Sample code	SSA (m^2/g)
F1	8.02
F10	24.2
untreated β-TCP	2.14
c-CaF_2	1.09

by treatment with fluoride-containing Ac-AcNa buffer solutions. In addition, the fluoride-treated β-TCP samples had larger SSAs than the untreated one (**Table 3**), indicating that this was due to the formation of F-HAp and CaF_2.

Figure 6(a) shows FE-SEM images of untreated β-TCP and fluoride-treated β-TCP samples. Untreated β-TCP exhibited an irregular morphology consisting of sintered micrometer-sized particles with smooth surface. F1 showed that sub-micrometer-sized rod-shaped F-HAp particles were distributed on the smooth surface of β-TCP particles. No characteristic morphology attributable to CaF_2 particles was observed in F1. In F10, sub-micrometer sized spherical CaF_2 particles had aggregated to form micrometer-sized particles resembling raspberries, and rod-shaped F-HAp particles were observed in the gaps between the spherical particles and beneath them.

Figure 6(b) shows cross-sectional images of a micrometer sized particle (F10) with the typical raspberry-like surface morphology. The following findings were observed in each area (A, B, C, D, and E): (A) A layer of sub-micrometer-sized spherical CaF_2 particles densely covered the surface; (C, E) Small hollow CaF_2 particles of different sizes were distributed beneath the CaF_2 particle layer, indicating that β-TCP dissolved after the CaF_2 particle layer had formed; and (B, D) Near the center of the micrometer-sized particle, aggregates of sub-micrometer-sized rod-shaped F-HAp particles with disordered orientations were observed. These results suggest the formation of a core–shell type structure consisting of F-HAp as the core and CaF_2 as the shell.

The formation of rod-shaped F-HAp and spherical CaF_2 particles is enhanced by a higher F^- concentration in the Ac-AcNa buffer solution. These two species are formed according to the following reactions:

Dissolution reaction (hydrolysis reaction)

$$\beta\text{-}Ca_3(PO_4)_2 \rightarrow 3Ca^{2+} + 2PO_4^{3-} \quad (2)$$

Precipitation reaction accelerated by fluoride

$$Ca^{2+} + 2F^- \rightarrow CaF_2\downarrow \quad (3)$$

$$10Ca^{2+} + 6PO_4^{3-} + xF^- + (2-x)H_2O \rightarrow Ca_{10}(PO_4)_6F_x(OH)_{(2-x)}\downarrow + (2-x)H^+ \quad (4)$$

Formation of disordered phase

$$PO_4^{3-} + H^+ \rightleftharpoons HPO_4^{2-} \quad (5)$$

$$PO_4^{3-} + H_2O \rightleftharpoons HPO_4^{2-} + OH^- \quad (6)$$

$$Ca^{2+} + HPO_4^{2-} \rightarrow CaHPO_4\downarrow \quad (7)$$

Overall reaction (dissolution–precipitation reaction) accelerated by fluoride.

$$4\beta\text{-}Ca_3(PO_4)_2 + 3xNaF + (2-x)H_2O \rightarrow Ca_{10}(PO_4)_6F_x(OH)_{(2-x)}\downarrow + (2-x)CaHPO_4\downarrow + xCaF_2\downarrow + 3xNa^+ + xPO_4^{3-} \ (0 < x < 2) \quad (8)$$

Based on Eq. (8), when $x = 1$, the molar ratio of F-HAp to CaF_2 is 1:1, which is consistent with the results of ^{19}F NMR analysis (Table 2).

The dissolution curves of the fluoride-treated and untreated β-TCP samples are shown in **Fig. 7**. The fluoride-treated β-TCP samples had lower initial dissolution rates than that of the untreated one (**Table 4**).

The dissolution efficiency was quantitatively evaluated:

$$D_e = \frac{\text{initial dissolution rate of fluoride-treated } \beta\text{-TCP}}{\text{initial dissolution rate of untreated } \beta\text{-TCP}} \quad (9)$$

D_e decreased in the following order: F1 > F10, indicating that the initial dissolution rate decreased on the β-TCP covered with amorphous CaF_2 and F-HAp particles (F1) and on core–shell type particles consisting of CaF_2 shell and F-HAp core (F10). The initial dissolution rate ($15.2\,mg{\cdot}dm^{-3}{\cdot}min^{-1}{\cdot}m^{-2}$) and SSA ($24.2\,m^2/g$) of F10 were very close to the previously reported dissolution rate ($13.0\,mg{\cdot}dm^{-3}{\cdot}min^{-1}{\cdot}m^{-2}$) and SSA ($27.0\,m^2/g$) for the fluoride-treated stoichiometric HAp sample (F1P0).[6] Since the dissolution rate of c-CaF_2 is extremely low (see Fig. 7), the initial dissolution rate of F10 is primarily governed by the dissolution of the F-HAp core.

Next, we investigated the effects of added PP ions on the dissolution–precipitation reaction products, which were formed by treating β-TCP particles with fluoride-containing Ac-AcNa buffer solutions.

Specifically, the XRD peaks corresponding to β-TCP (ICDD-PDF #00-09-0169) decreased in intensity in the

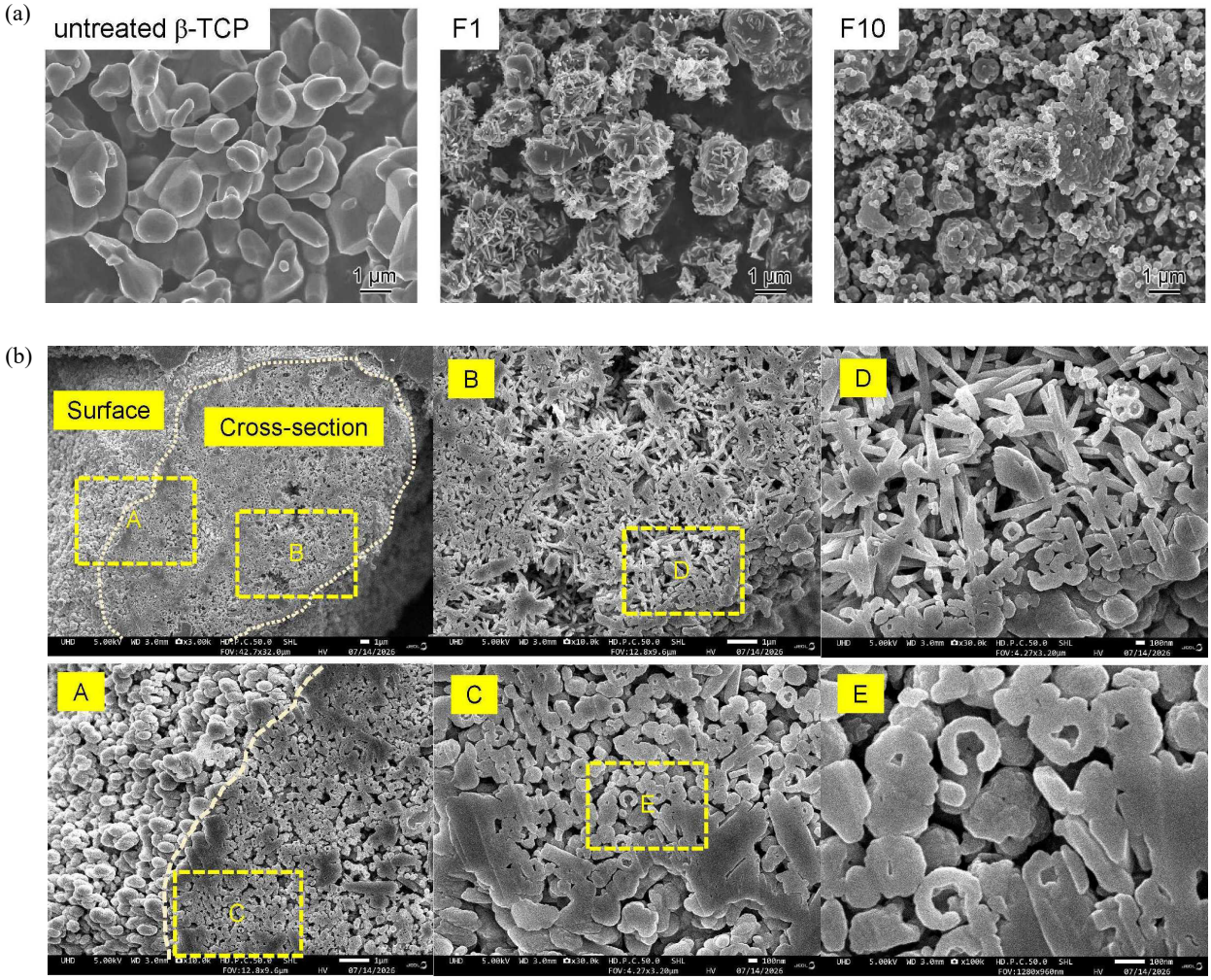


Fig. 6. (a) FE-SEM images of the hydrolysis products of β-TCP treated with fluoride-containing Ac-AcNa buffer solutions. (b) Cross-sectional FE-SEM images of a micro-meter sized particle (F10) with a surface morphology resembling raspberries.

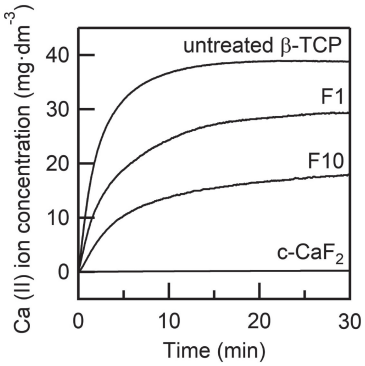


Fig. 7. Ca(II) ion dissolution curves of the fluoride-treated and untreated β-TCP samples in Ac-AcNa buffer solutions. For comparison, the Ca(II) ion dissolution curve of c-CaF_2 was also shown.

following order: P10F10 > P1F10 > P0.1F10 > P0.01F1 > P0.001F10 > P0F10, while those corresponding to HAp (ICDD-PDF#00-09-0432) and CaF_2 (ICDD-PDF#00-35-0816) were observed in P0.001F10, and P0F10 (**Fig. 8**).

Table 4. Initial dissolution flux of the fluoride-treated and untreated β-TCP samples in Ac-AcNa buffer solutions

Sample code	Initial dissolution flux (mg·m^{-3}·min^{-1})	Initial dissolution rate (mg·dm^{-3}·min^{-1}·m^{-2})	D_e
F1	9.06	113	0.115
F10	3.68	15.2	0.0154
Untreated β-TCP	21.1	986	—
c-CaF_2	0.02	1.99	—

At PP ion concentrations of 0.01 mmol·dm^{-3} or less, the SSA of the specimens increased significantly. On the other hand, when the PP ion concentrations was within 0.01–10 mmol·dm^{-3}, the SSA was close to that of untreated β-TCP (2.14 m^2/g) (**Fig. 9**). These results indicate that the addition of PP ions to fluoride-containing Ac-AcNa buffer solutions inhibited not only the hydrolysis reaction of β-TCP [Eq. (2)] but also the formation of F-HAp and CaF_2 [Eq. (3) and Eq. (4)]. The SSA values of P0F0 and P10F0 (2.64 and 2.43 m^2/g, respectively) are larger than that

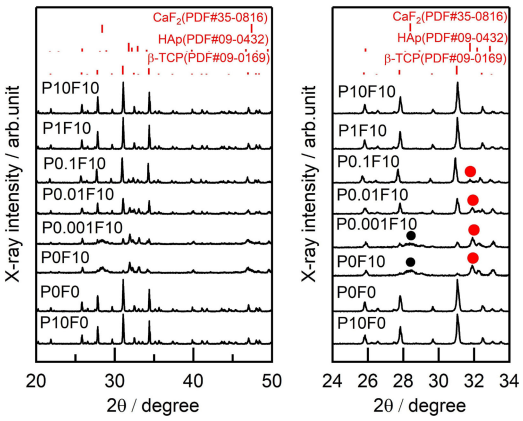


Fig. 8. XRD patterns of the hydrolysis products of β-TCP treated with Ac-AcNa buffer solutions containing fluoride and various concentrations of PP ions. For comparison, XRD patterns of P0F0 and P10F0 are also shown. red circle: HAp, black circle: CaF_2.

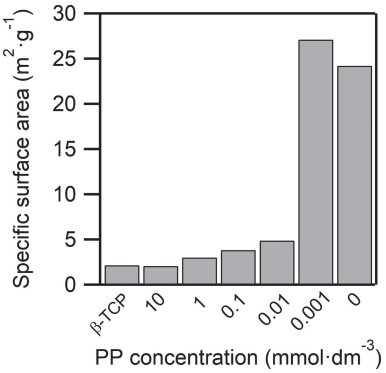


Fig. 9. SSA of PyF10 ($y = 0.01$ and 10) samples as a function of the PP ion concentration.

of untreated β-TCP. This indicates that the hydrolysis reaction of β-TCP [Eq. (2)] proceeded more slowly in fluoride-free buffer solutions than in fluoride-containing one, resulting in a smaller particle size of β-TCP without the precipitation of HAp and CaF_2.

The dissolution curves of fluoride-treated and untreated β-TCP samples are shown in **Fig. 10**. The initial dissolution rate of the fluoride-treated one was lower than that of the untreated β-TCP (**Table 5**). The initial dissolution rates of P10F0 and P10F10 were approximately half that of untreated β-TCP but still more than 28 times faster than that of P0F10. The addition of PP ions to the fluoride treatment solution suppressed the formation of CaF_2 and F-HAp particles, resulting in a lower acid resistance of the reaction products obtained through fluoride treatment of β-TCP particles.

Consequently, the formation of CaF_2 and F-HAp particles is necessary to enhance the acid resistance of the reaction products.

Structural models of β-TCP treated with fluoride-containing Ac-AcNa buffer solutions are shown in **Fig. 11**. In an acidic solution with a high fluoride concentration (F10), sub-micrometer-sized spherical CaF_2

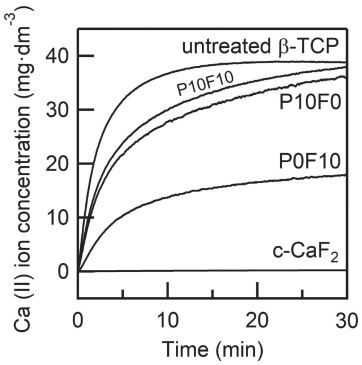


Fig. 10. Ca(II) ion dissolution curves of the hydrolysis products of β-TCP treated with Ac-AcNa buffer solutions containing fluoride and various concentration of PP ions, namely the PyF10 ($y = 0$ and 10) samples. For comparison, the Ca(II) ion dissolution curve of P10F0 was also shown.

Table 5. Initial dissolution flux of the hydrolysis products of β-TCP treated with Ac-AcNa buffer solutions containing fluoride and various concentrations of PP ions

Sample code	Initial dissolution flux ($mg \cdot dm^{-3} \cdot min^{-1}$)	Initial dissolution rate ($mg \cdot dm^{-3} \cdot min^{-1} \cdot m^{-2}$)
P0F10	3.68	15.2
P10F10	11.7	568
P10F0	10.3	423
Untreated β-TCP	21.1	986
c-CaF_2	0.02	1.99

particles precipitate preferentially, forming raspberry-like aggregates (namely CaF_2 particle layer) that cover the β-TCP surface [Step 1: see Fig. 6(b)D]. At the interface between β-TCP and the CaF_2 particle layer, the formation of CaF_2 particles reduces the fluoride ion concentration, inducing the nucleation and growth of rod-shaped F-HAp particles. [Step 2: see Fig. 6(b)C]. Finally, a core–shell-type structure with F-HAp core and CaF_2 shell is formed (Step 3). The hydrolysis reaction of β-TCP proceeds throughout both steps, and it could be accelerated by the formation of sub-micrometer-sized spherical CaF_2 particle layer and aggregates of randomly oriented, sub-micrometer-sized rod-shaped F-HAp particles.

4. Conclusions

Commercially available β-TCP was treated with a fluoride-containing aqueous solution of Ac-AcNa buffered at pH 5.5. XRD, SEM and NMR analysis confirmed the deposition of F-HAp and CaF_2 on β-TCP after fluoride treatment, indicating that both Ca^{2+} and PO_4^{3-} ions released from β-TCP combined with F^- in the solution to form a core–shell-type structure with F-HAp core and CaF_2 shell. Adding PP ions to the fluoride treatment solution inhibited not only the hydrolysis reaction of β-TCP but also the formation of F-HAp and CaF_2.

Dissolution–precipitation products (namely F-HAp and CaF_2) formed during fluoride treatment of β-TCP particles

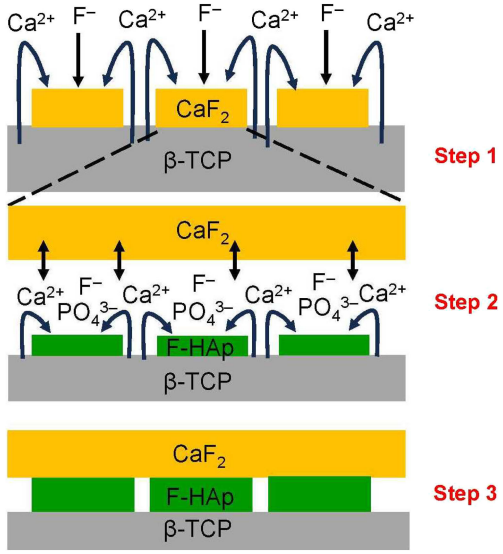


Fig. 11. Structural models of β-TCP treated with fluoride-containing Ac-AcNa buffer solutions. Step 1: CaF_2 precipitation, Step 2: F-HAp formation at the interface between β-TCP and CaF_2. The hydrolysis reaction of β-TCP proceeds throughout both steps.

reduced the particles' initial dissolution rate in Ac-AcNa buffer solutions. The addition of PP ions to the fluoride treatment solution suppressed these two products, resulting in reduced acid resistance for the treated β-TCP particles.

Acknowledgements This study was partially supported by a Grant-in-Aid for Scientific Research (B) from the Japan Society for the Promotion of Science (24360274) and JSPS Program for Forming Japan's Peak Research Universities (J-PEAKS) Grant Number JPJS00420230010.

References

1) J. D. B. Featherstone, *Community Dent. Oral* 27, 31 (1999).
2) S. R. Grobler, B. Øgaard and G. Rølla, Uptake and retention of fluoride in sound dental enamel in vivo after a single application of neutral 2 % sodium fluoride, in "Tooth Surface Interactions and Preventive Dentistry", Ed. by G. Rølla, T. Sønjju and G. Embery, IRL Press, London (1981) pp. 17–26.
3) G. Rølla and B. Øgaard, Studies on the solubility of calcium fluoride in human saliva, in "Factors Relating to Demineralization and Remineralization of the Tooth", Ed. by S. A. Leach, IRL Press, Oxford (1986) pp. 45–50.
4) J. Christoffersen, M. R. Christoffersen, W. Kibalczyc and W. G. Perdok, *Acta Odontol. Scand.* 46, 325 (1988).
5) B. Øgaard, *Caries Res.* 35[Suppl. 1], 40 (2001).
6) S. Hayakawa, Y. Okada and T. Yoshioka, *J. Ceram. Soc. Jpn.* 133, 15 (2025).
7) H. Fleisch and S. Bisaz, *Nature* 195, 911 (1962).
8) T. V. Vasudevan, P. Somasundaran, C. L. Howie-Meyers, D. L. Elliot and K. P. Ananthapadmanabhan, *Langmuir* 10, 320 (1994).
9) Z. Amjad, *Langmuir* 7, 600 (1991).
10) D. Massiot, F. Fayan, M. Capron, I. King, S. Le Calve, B. Alonso, J. O. Durand, B. Bujoli, Z. Gan and G. Hoatson, *Magn. Reson. Chem.* 40, 70 (2002).
11) S. Hayakawa, K. Ando and T. Yoshioka, *J. Ceram. Soc. Jpn.* 134, 31 (2026).
12) M. Bohner, J. Lemaitre and T. A. Ring, *J. Colloid Interf. Sci.* 190, 37 (1997).
13) J. S. Bow, S. C. Liou and S. Y. Chen, *Biomaterials* 25, 3155 (2004).
14) S. Koutsopoulos, *J. Biomed. Mater. Res.* 62, 600 (2002).
15) M. Jarlbring, D. E. Sandström, O. N. Antzutkin and W. Forsling, *Langmuir* 22, 4787 (2006).